J Solid State Electrochem (2011) 15:349–356
DOI 10.1007/s10008-010-1260-0

ORIGINAL PAPER

NMR investigations on the lithiation and delithiation of nanosilicon-based anodes for Li-ion batteries

Jan-Henning Trill · Chuangqi Tao · Martin Winter · Stefano Passerini · Hellmut Eckert

Received: 12 November 2010 / Revised: 22 November 2010 / Accepted: 24 November 2010 / Published online: 22 December 2010

Abstract Lithiation and delithiation of nanosilicon anodes of 100–200 nm diameter have been probed by ex situ solid-state high-resolution ^{7}Li nuclear magnetic resonance (NMR) and transmission electron microscopy (TEM) methods. Samples were charged within pouch cells up to capacities of 1,500 mAh/g at 0.1 C, and subsequently discharged at the same rate. The NMR spectra reveal important quantitative information on the local lithium environments during the various stages of the charging/discharging process. The TEM experiments show that the electrochemical lithiation of nanosilicon particles results in core-shell materials, consisting of Li_xSi shells surrounding a core of residual silicon. The NMR spectra yield approximate Li/Si ratios of the lithium silicides present in the shells, based on the distinct local environments of the various types of ^{7}Li nuclei present. The combination of NMR with TEM gives important quantitative conclusions about the nature of the electrochemical lithiation process: Following the initial formation of the solid electrolyte interphase layer, which accounts for an irreversible capacity of 240 mAh/g, lithium silicide environments with intermediate Li concentrations ($Li_{12}Si_7$, Li_7Si_3, and $Li_{13}Si_4$) are formed at the 500 to 1,000 mAh/g range during the charging process. At a certain penetration depth, further lithiation does not progress any further toward the interior of the silicon particles but rather leads to the formation of increasing amounts of the lithium-richest silicide, $Li_{15}Si_4$-type environments. Delithiation does not result in the reappearance of the intermediate-stage phases but rather only changes the amount of $Li_{15}Si_4$ present, indicating no microscopic reversibility. Based on these results, a detailed quantitative model of nanophase composition versus penetration depth has been developed. The results indicate the power and potential of solid-state NMR spectroscopy for elucidating the charging/discharging mechanism of nano-Si anodes.

Introduction

While lithium-ion batteries are well-established energy storage systems of considerable commercial interest, future applications of such materials for electric mobility require significant improvements in capacity, reversibility, and transport behavior. Current research efforts focus on the development of new materials and formulations for all the constituent electrochemical cell components, including anode and cathode, as well as electrolyte systems. In this connection, replacement of currently used carbon-based anode materials by silicon-based systems has attracted lots of interest, based on its theoretical charge capacity of 3,570 mAh/g compared to graphite (372 mAh/g). However, the reversibility of the charging and discharging process is poor. While a number of crystalline lithium silicides such as $Li_{12}Si_7$, Li_7Si_3, $Li_{13}Si_4$, $Li_{15}Si_4$, and $Li_{21}Si_5$ [1–8] are accessible through thermal synthesis routes, electrochemical lithiation so far has only resulted in amorphous Li_xSi material [9]. Obrovac [10] reported that amorphous Li_xSi phase transformed into a crystalline metastable $Li_{15}Si_4$ when the voltage is lower than 50 mV (vs. Li/Li^+) during lithiation. Similar results were also reported by Dahn et al.

Dedicated to Professor Robert Schöllhorn on the occasion of his 75th birthday

J.-H. Trill · C. Tao · M. Winter · S. Passerini · H. Eckert (✉)
Institut für Physikalische Chemie,
Westfälische Wilhelms-Universität Münster,
Corrensstrasse 30,
48149, Münster, Germany
e-mail: eckerth@uni-muenster.de

[11], where $Li_{15}Si_4$ was observed below 30 mV (Li/Li^+) in both crystalline and amorphous Si films thicker than 2 μm. However, in both studies, the amorphous Li_xSi phase and the phase change were not observable by X-ray powder diffraction. An alternative method for structural studies of amorphous or poorly crystalline materials is solid-state nuclear magnetic resonance (NMR) spectroscopy, which is an element-selective, inherently quantitative method particularly sensitive to local atomic (short-range order) environments. During the past 15 years, much of the focus of such NMR studies has been on the lithiation of carbon-based anode materials [12]. Dedryvère et al. reported the lithiation process when Li-metal alloys dispersed in an amorphous matrix of lithium sulfide at low potentials by using ^{7}Li NMR [13]. Other works have been done to reveal the properties of the solid/electrolyte interphase (SEI) passivating layer on the surface of electrodes which arises from the reductive decompositions of a small amount of organic electrolyte [14, 15]. A major step in the understanding of silicon-based anodes was achieved through the in situ NMR study of the lithiation of silicon [16, 17]. The ^{7}Li resonances of the known crystalline lithium silicides have distinguishable NMR shifts and can thus be utilized to determine the composition of the anode material by postmortem and even in situ characterization. In this study, we combine the charge profiles of Li-ion batteries with the compositional information derived from $^{6/7}$Li NMR to learn about the microscopic transformations involved in the lithiation and delithiation of silicon/Li_xSi anodes

Experimental

Anode preparation Eight weight percent NaCMC (Sigma Aldrich, USA), 15 wt% Super-P (Timcal, Switzerland), and 77 wt% nano-Si (Evonik Degussa GmbH, Germany, particle size 100–200 nm) were added into water and dispersed by using Scandex Disperser DAS 200 (Lau GmbH, Germany) for 1 h (with additional ZrO_2 balls as dispersing media). The obtained homogenous slurry was then filtered and evacuated under 20 mbar while stirred with a magnetic stirrer for 30 min. The slurry was cast on the copper foil with a blade coater, the height of which was adjusted to 100 μm. The coated electrode tape was dried at 80 °C for 0.5 h and then at 110 °C for 2 h. Pieces of 5 cm× 5 cm were cut from the electrode tape and further dried at 130 °C under vacuum for 10 h.

Battery assembly The anodes were assembled in pouch cells composed with a commercial cathode material (5.2 cm×5.2 cm, Litarion™, Evonik GmbH, Germany). Celgard 2320 (Celgard, USA) was used as separator, and DG-2 (1 M $LiPF_6$ in EC:EMC=1:1 by weight, Ferro Corporation, USA, with the addition of 2 wt% vinylene carbonate) was used as electrolyte. The cell was sealed under vacuum. The pouch cells were tested in a constant current-constant voltage protocol (CCCV) between 3.0 and 4.2 V cutoff voltages using a Maccor S4000 Battery Tester (MACCOR Ltd., USA). In the first cycle, the charge rate was 0.1 C until the voltage reached 4.2 V (CC step) and held until the specific capacity was reached (CV step); the discharge rate was 0.1 C until the 3.0 V (CC step only). The charge and discharge rates were set at 0.5 C for all the subsequent cycles. Six pouch cells were prepared for the MAS-NMR analysis as follows: Sample C-500 was lithiated to 500 mAh/g, sample C-1000 to 1,000 mAh/g, and sample C-1500 to 1,500 mAh/g. Sample D-1000 was obtained by delithiation to 1,000 mAh/g and sample D-400 by full delithiation to yield a residual (irreversible) capacity of 400 mAh/g. Sample CC-950 was first charged to 1,500 mAh/g, then fully discharged, and once again recharged up to a total capacity of 950 mAh/g. $LiCoO_2$ was used as source-sink material for lithium.

NMR spectroscopy For ex situ NMR analysis, the pouch cells were disassembled under inert conditions in a glove box (MBRAUN, Germany), and the anode material was removed from the copper current collector. After rinsing with dimethylene chloride (DMC), the samples were dried under vacuum at room temperature for 4 h. About 20 mg of sample were placed in 4-mm high-speed ZrO_2 rotors for NMR measurements. Experiments were carried out on a Bruker DSX400 spectrometer at spinning speeds between 10,000 and 15,000 Hz. The ^{7}Li NMR spectra were recorded at 155.56 MHz with typically 1,024 scans with a 30° single pulse of 0.8 μs length and a recycle delay of 0.5 s. ^{6}Li spectra were recorded at 58.09 MHz using typically 1,024 scans with 30° pulses of 2.1 μs length and a recycle delay of 5 s. Chemical shifts are reported relative to a 1 M aqueous solution of lithium chloride. ^{29}Si spectra were taken on a Bruker DSX-500 NMR spectrometer operating at 99.54 MHz, using 90° pulses of 4.2 μs length and relaxation delays varying between 1 and 60 s. Thirty-two thousand scans had to be acquired to achieve decent signal-to-noise ratios. Chemical shifts are quoted relative to liquid tetramethylsilane.

Electron microscopy Scanning electron microscopy (SEM) was conducted on an EVO® MA 25 instrument (Carl Zeiss SMT AG, Germany). For TEM, the sample CC-950 was dispersed in DMC (dimethyl carbonate), and a small droplet of the dispersion was dripped on the surface of a 3.05-mm-diameter Cu grid (200 mesh) with 10 nm (thickness) carbon layer. The sample was kept in the glove box and dried

under vacuum at room temperature, before it was transferred under argon into the microscope. The TEM measurement was carried out on a Libra 200FE (Carl Zeiss SMT, Germany) instrument. The accelerating voltage was 200 kV.

Results

Solid-state NMR studies Figure 1 shows the six samples of Li_xSi-containing anode material and their respective lithiation stages during the electrochemical lithiation cycles as described above. The corresponding voltage–capacity curves are given in Fig. 1. Here, it can be observed that the voltage of the pouch cell quickly increased to 3.6 V during the first 100 mAh/g of charge. A much more gentle voltage slope was observed afterward, with a gradual voltage increase from 3.6 to 4.2 V, where a final capacity of 1,500 mAh/g was reached. The first cycle irreversible capacity (29.5%, about 400 mAh/g), which mainly originates from SEI formation, is easily correlated with the amount of lithium that could not be extracted from the Si electrode during discharge (delithiation).

As already reported in the literature, NMR can very well distinguish between lithium in different crystalline lithium silicides [16]. Our own NMR investigations reveal that the ^{7}Li NMR resonances of these compounds can be fitted by single Gauss–Lorentz lineshapes, that reflect motional averaging of the various lithium sites present in these materials. In general agreement with the results of Grey and coworkers [16], we found these signals to appear at the following resonance shifts: $Li_{12}Si_7$ at 18.5 ppm, Li_7Si_3 at 16.5 ppm, $Li_{13}Si_4$ at 11 ppm, and $Li_{15}Si_4$ at 6 ppm [19]. Figure 2 shows the spectra of the amorphous Li_xSi anode

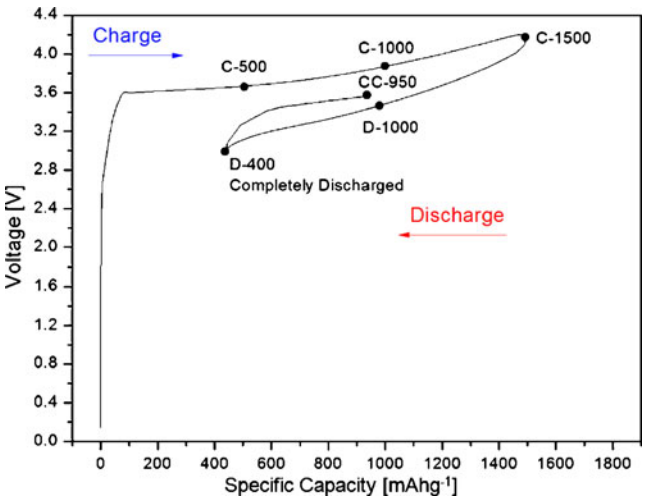

Fig. 1 Voltage vs. specific capacity plot of the cells containing nano-Si anodes during cycling. The *marked points* identify the lithiation states of the Si samples characterized

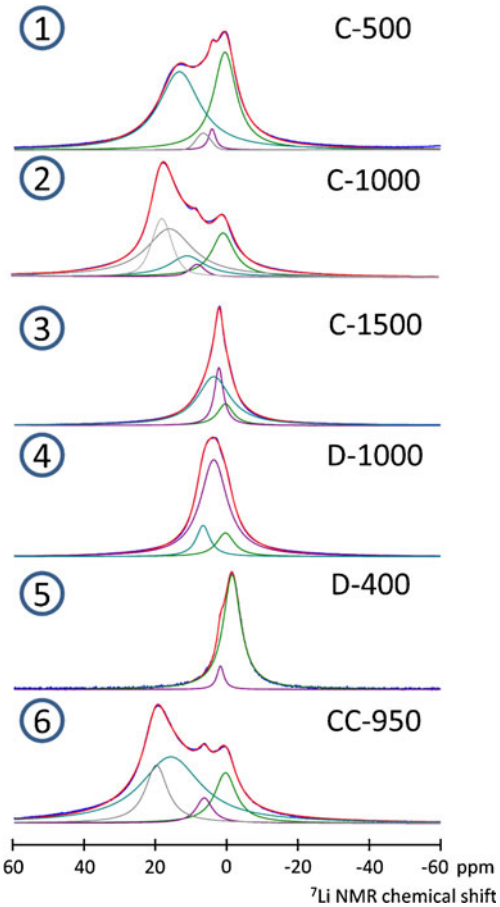

Fig. 2 ^{7}Li MAS-NMR spectra at room temperature of the six samples investigated. The spectra have been simulated (*red curves*), and the individual components are shown for each spectrum

samples representing the different charging states. They consist of distinct resonances with chemical shifts in the vicinity of those of the above crystalline compounds, suggesting that despite the amorphous character of the samples, distinct local lithium environments can be identified that resemble those of the above-mentioned crystalline reference materials. In addition, ^{7}Li NMR signals near 0 ppm are attributed to ionic species (LiF, Li_2O, Li_2CO_3), e.g., formed at the solid-electrolyte interface. Based on Fig. 2, the charging and discharging processes can be described as follows:

Initial lithiation At the beginning of the lithiation process (sample C-500), the formation of the SEI layer is indicated by the ^{7}Li resonance at 0 ppm. In addition, a broad signal near 16 ppm is observed, suggesting the presence of lithium in similar environments as found in Li_7Si_3. Based on the large linewidth of this resonance, it is possible that lithium ions in $Li_{12}Si_7$-like environments also contribute to this signal. As lithiation progresses toward sample C-1000, the strong contribution from $Li_{12}Si_7$-type environments

becomes clearly evident by an intense signal near 18 ppm. Furthermore, a broad signal near 13 ppm of considerable intensity is observed, suggesting a substantial contribution due to $Li_{13}Si_4$-like environments.

At the maximum lithiation level in the investigated series (C-1500), the resonances above 10 ppm have completely disappeared. Instead, an asymmetric lineshape centered near 5 ppm is observed, suggesting that lithium ions are now dominantly present in $Li_{15}Si_4$-like environments. Figure 2 indicates that the lineshape can be artificially deconvoluted into a narrower and a broader component having slightly different chemical shifts. However, it is also possible that there is a continuous distribution of resonance frequencies indicating a range of local to $Li_{15}Si_4$ environments in different stages of ordering.

Delithiation Upon delithiation by about 500 mAh/g (D-1000), only subtle spectral changes are observed, with a minor change in the center of gravity toward higher frequency. We also attribute this signal to a range of $Li_{15}Si_4$-like local environments. As expected, the amplitude of this signal is significantly decreased, making it possible to observe the shoulder near 0 ppm attributed to ionic species in the SEI layer more clearly. Most importantly, however, this spectrum differs significantly from that of sample C-1000 observed at the same lithiation stage during charging. Specifically, lithium environments typical of $Li_{12}Si_7$, Li_7Si_3, or $Li_{13}Si_4$ do not (re-)appear during the delithiation process, indicating that there is no microscopic reversibility. The remarkable differences between the lithium environments observed at comparable charging states in the lithiation and the delithiation direction imply that charging the sample to 1,500 mAh/g produces an irreversible change in the sample, resulting in a different lithium distribution along the discharging process. Finally, the fully delithiated sample, which corresponds to a charging state of about 400 mAh/g (D-400), shows a dominant ^{7}Li NMR resonance at 0 ppm, which can be assigned to the SEI. In addition, some lithium in $Li_{15}Si_4$-like environments is present, from which lithium cannot be removed anymore. Again, there is no evidence of lithium silicide local environments with lower Li/Si ratios as were observed during the lithiation process.

Second lithiation The ^{7}Li NMR spectrum of sample CC-950, which was relithiated to a charging state of 950 mAh/g, is similar to that of sample C-1000. This indicates that after the formation of the irreversible part of the SEI, a similar lithiation process occurs during the second cycle. Also, during the second cycle, no preference for direct transformation of the material to $Li_{15}Si_4$ is observed.

For further confirmation of the above findings, additional ^{6}Li NMR spectra were obtained on samples C-1500 to CC-950 (labeled 3–6), leading to the results summarized in Fig. 3. The detection sensitivity for ^{6}Li is substantially lower compared to that of ^{7}Li, owing to longer spin–lattice relaxation times, lower natural abundance, and the smaller size of the ^{6}Li magnetic moment. Nevertheless, the latter two aspects often result in significantly improved resolution compared to ^{7}Li MAS-NMR as the homonuclear dipole–dipole interaction strengths (which are known to dominate MAS-NMR linewidths in crystalline lithium compounds) are significantly attenuated. Furthermore, ^{6}Li MAS-NMR spectra are not complicated by spinning sidebands arising from first-order quadrupolar broadening of other Zeeman transitions ("satellites"). Figure 3 illustrates that in the present samples, these benefits are only partially realized, suggesting that the MAS-NMR lineshapes are dominated by chemical shift distribution effects. Still, the distinct lineshape component arising from the ionic lithium environments present in the SEI are generally better resolved in the ^{6}Li MAS-NMR spectra, simplifying the quantification of individual lineshape components. In the spectra of samples C-1500, D-1000, and D-400, the "SEI" Li content is found to be about 16%, 22%, and 58%, respectively, consistently indicating that the irreversible capacity loss corresponds to 240±10 mAh/g for each sample. Table 1 summarizes the ^{6}Li chemical shifts and fractional areas obtained by peak deconvolution into up to five Gauss–Lorentz components. In cases of samples C-500 and C-1000, for which no ^{6}Li MAS-NMR spectra were available, the peak deconvolution was done on the ^{7}Li MAS-NMR

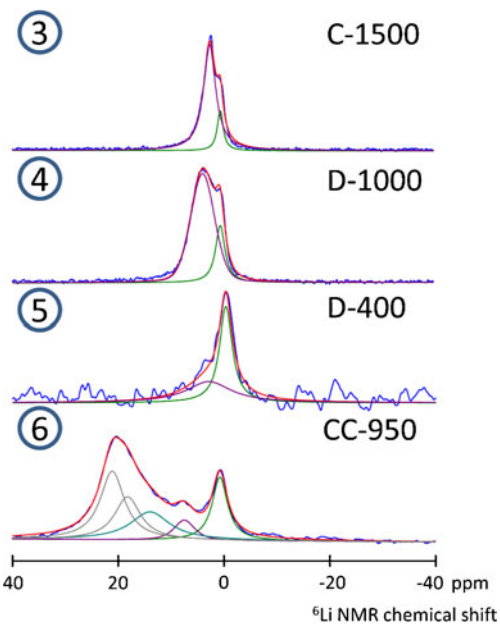

Fig. 3 ^{6}Li MAS-NMR spectra at room temperature of samples C-1500, D-1000, D-400, and CC-950. The spectra have been simulated (*red curves*), and the individual components are shown for each spectrum

Table 1 Chemical shifts and fractional areas of the individual components in the ^{6}Li MAS-NMR lineshape deconvolutions of the samples under study

Sample	mAh/g	$Li_{12}Si_7$		Li_7Si_3		$Li_{13}Si_4$		$Li_{15}Si_4$		SEI	
		δ_{iso} (ppm)	A (%)	δ_{iso} (ppm)	A (%)	δ_{iso} (ppm)	A (%)	δ_{iso} (ppm)	A (%)	δ_{iso} (ppm)	A (%)
C-500	500			14*	48*			7*, 4*	11*	0.5*	41*
C-1000	1,000	18*	21*	16*	37*	11*	16*	8*	4*	0.5*	22*
C-1500	1,500							3	84	0.5	16
D-1000	1,000							4	78	0.5	22
D-400	400							3	42	−0.4	58
CC-950	950	21	32	18	21	14	21	7	7	0.8	19
C-1000H	1,000			16.4±0.5	29	12	33	3	14	0.7	23

For samples C-500 and C-1000, the deconvolution results refer to the ^{7}Li MAS-NMR spectra. Experimental uncertainties are ±1 ppm for chemical shift and ±5% for fractional areas

spectra (indicated by asterisks in Table 1). For those samples where both ^{6}Li and ^{7}Li MAS-NMR spectra were available, the peak deconvolution results were generally found to be consistent, with minor variations of peak positions and areas for the individual Li_xSi-phase components. Owing to the somewhat better resolution observed in ^{6}Li MAS-NMR, all subsequent analysis was done on the ^{6}Li NMR peak deconvolution results summarized in Table 1.

Figure 4 shows the effect of sample heating following a variable temperature study (not shown) on sample C-1000. After sample exposure at 440 °C for about 1.5 h, the spectrum indicates an irreversible change of the sample, and the strong sharp resonance at 16.4 ppm suggests the formation of crystalline Li_7Si_3 following this thermal treatment. Furthermore, it is interesting to note that before heating, no ^{29}Si spectrum of the sample could be observed in a 12-h experiment, whereas after heating, only 4 h were sufficient to acquire a rather sharp ^{29}Si line with a chemical shift of 364 ppm. The assignment of this signal is not certain at the present time. Similar annealing studies carried out on the C-1500 sample (data not shown) reveal no significant change of the ^{7}Li MAS-NMR spectrum.

Electron microscopy Figure 5 shows the SEM of the Si particles in different magnifications used in this study. From Fig. 5a, it can be observed that the silicon particles possess a spherical shape and mainly occur in the form of aggregates. It can also be seen from Fig. 5b that the primary particle size of the silicon spheres is in the range between 100 and 200 nm. Figure 6 shows the TEM images (a, bright field and b, dark field) as well as the selected area electron diffraction (SAED) patterns (inset of a) of representative particles of the CC-950 anode material. These pictures show an agglomeration of some Li_xSi nanoparticles with about 150 to 200 nm diameter. While many particles

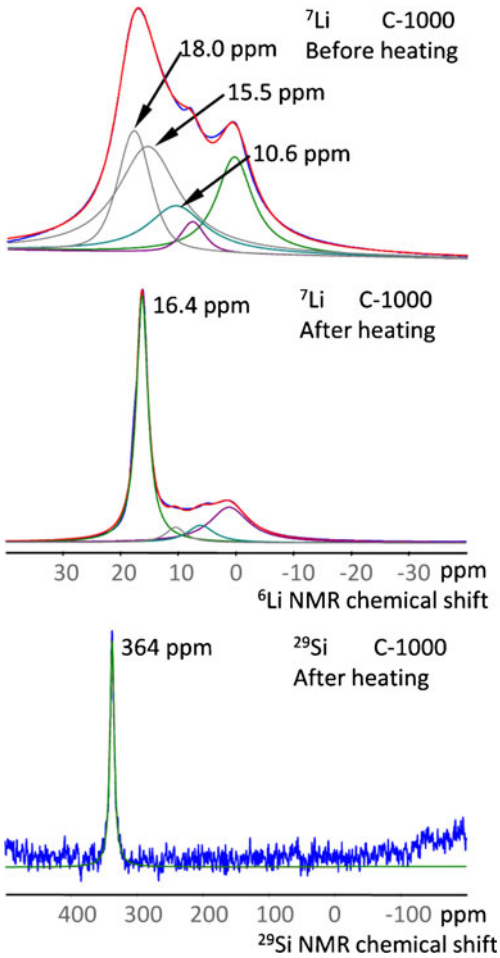

Fig. 4 ^{7}Li MAS-NMR spectra of sample 2 (C-1000) before (*top*) and after (*middle*) sample heating to 440 °C for 1.5 h. The spectra have been simulated (*red curves*), and the individual components are shown for each spectrum. ^{29}SI NMR spectrum after heating (*bottom*)

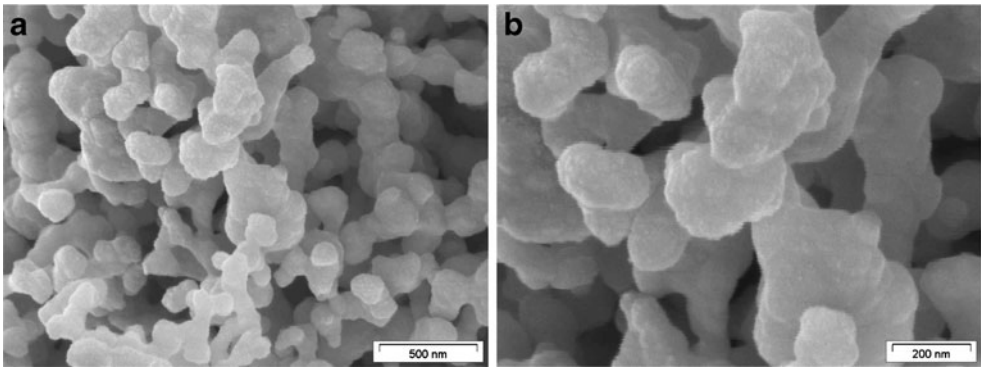

Fig. 5 Scanning electron micrographs of Si active material in different resolutions. **a** 500 nm. **b** 200 nm

overlap in the direction of the observation axis, the center of the picture shows a sphere, seemingly in loose contact with its neighbors, which has limited overlap and thus serves as a good probe to study the structure of the nano-Li_xSi spheres.

The sphere consists of three major parts: First, a core of about 120 nm diameter, which appears dark in the bright field; second, a rather transparent shell of about 30–40 nm thickness, and finally, a surface layer with varying thicknesses between 5 and 10 nm. The dark field image (Fig. 6b), which was taken at the reflection, marked in the inlet of Fig. 6a, shows a strong signal from the particles' core. This reflection belongs to one of the three rings, created by discrete spots, which are characteristic for the (111), (220), and (311) planes of crystalline silicon. This indicates the purity and crystalline structure of the core. However, as indicated by the reflections of the surrounding particles, a polycrystalline nature of the nanosilicon cores seems much more abundant. The core is mainly surrounded by a rather transparent phase, which does not show crystalline reflections anywhere in the SAED picture, thus suggesting that this shell is rather amorphous. A very close look might indicate a slight difference of intensity between the outer and inner part of this shell, but we do not consider this indication strong enough to identify two separable phases. We attribute the shell to Li_xSi phases, probably with varying Li concentration. On the surface of the particle, we find porous areas (marked by solid ellipses in a) which are part of the outer layer. It is likely that what is seen here represents the SEI, where Li-containing compounds can be found. The density in this phase is even less than within the shell.

Discussion

From the data presented above, in particular the results of the NMR and TEM analysis, it is clearly suggested that the lithiation process of Si anodes with a charging rate of 0.1 C is characterized by a nonuniform transformation of the material. To evaluate the NMR shifts, one has to keep in mind that all the Li_xSi phases detected exist in the outer 30–40-nm shell of the former silicon nanoparticles. This and the absence of diffraction signals other than from crystalline silicon indicate that no long-range ordering can be found. Thus, we can expect to see some deviations and variations of the lithium NMR resonance shifts of this anode material

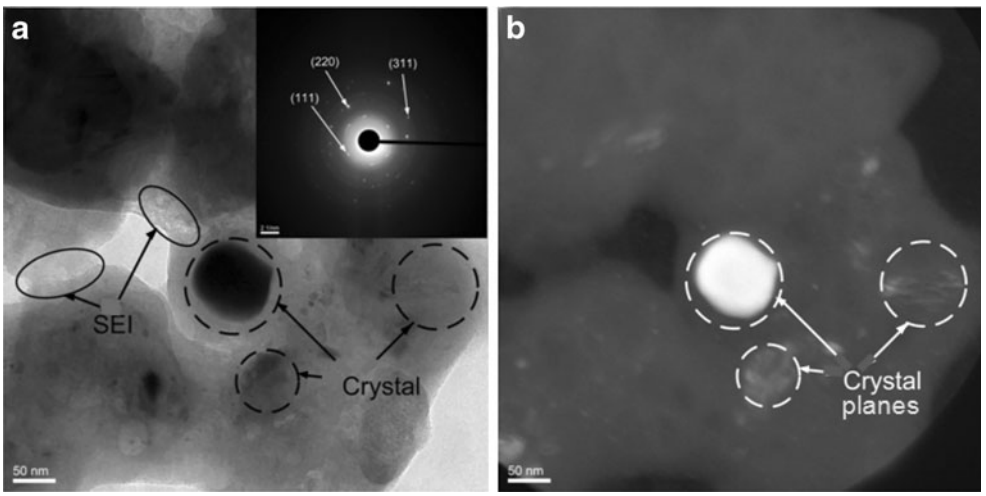

Fig. 6 **a** Bright field high-resolution transmission electron microscopy picture of a Si particle from sample CC-950 and SAED patterns (*inset*). **b** Dark field TEM picture of a Si particle from sample CC-950

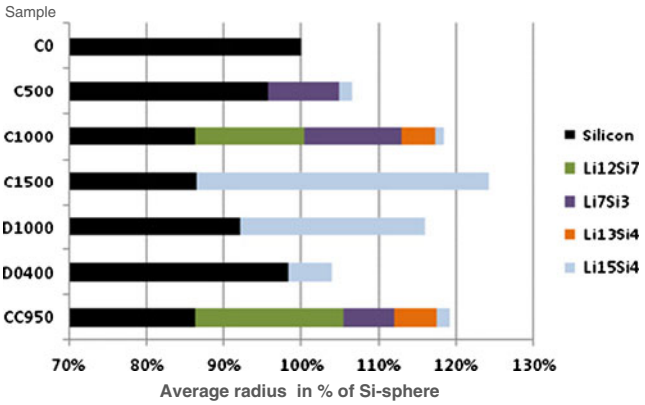

Fig. 7 Quantitative distribution of lithium environments during the lithiation–delithiation cycle of nano-Si as deduced from this study. This model is based on the simplified assumption that the nanosilicon particles have spherical symmetry and are penetrated from the outside by lithium, which leads to an overall expansion of the spherical particles. The values given represent the radius of the particles in percent of that of Si before lithiation

from those observed for crystalline lithium silicides. From the TEM images, it can be observed that the silicon nanoparticles of the lithiated anode material consist of three parts: (1) a crystalline silicon core, (2) a Li_xSi shell, and (3) a "SEI" surface layer. In the light of this, the interpretation of $^{6/7}$Li NMR spectra now allows for a more detailed view of these three parts. Since the intensities of the NMR signals are quantitatively proportional to the number of lithium atoms in the corresponding environments, combining this distribution with the total charge density of the sample allows us to determine the fraction of charge density invested in each of these environments. From there, the fraction of converted and unconverted silicon can be determined. In the final step, based on the silicon densities in the Li_xSi phases and assuming a spherical symmetry of the particles, a radial distribution of the phases in the particle can be modeled.

The first finding of this analysis is that the charge density represented by the 0.5-ppm resonance is constant throughout the set of samples, and equal to 240±10 mAh/g. In the next step, the silicon content of the Li_xSi phases can be determined, where the fraction of silicon in a Li_xSi component P divided by all silicon simply equals: $Si(P) = \rho(P)/\rho_{max}(P)$, where $\rho(P)$ is the relative charge density of the component P as determined from the samples above, and $\rho_{max}(P)$ is the theoretical charge density of this phase (e.g. $\rho_{max}(Li_{15}Si_4)$=3,579 mAh/g). The fraction of silicon remaining in the particle core, Si(C), then is calculated by balance: $Si(C) = 1 - \Sigma Si(P)$, excluding the charge density in the SEI layer.

Now, based on the volume per silicon atom (V_{Si}= 20.0 Å^3/Si, $V_{Li12Si7}$=58.0 Å^3/Si, V_{Li7Si3}=51.5 Å^3/Si, $V_{Li13Si4}$=67.3 Å^3/Si, and $V_{Li15Si4}$=71.7 Å^3/Si) [20], the radial distribution of the particles can be modeled. Here, three assumptions are critical: (1) The lithium penetration of the spherical particles also has a spherical symmetry, (2) the Li concentration gradient decreases toward the particles' core, and (3) the NMR resonances, which do not exactly correspond with a signal of a pure Li_xSi phase, can be roughly ascribed to one of the neighboring phases without generating much inaccuracy. We believe that the latter assumption is reasonable since the lithium content of potential neighboring phases never differs by more than 7 percentage points.

Following the conversion of the relative volumes into the relative shell radii with $r_{out}(Li_xSi) = [V(Si(C)) + \Sigma V(Si(P))]^{1/3}$ where $\Sigma V(Si(P))$ is the sum of the volumes of all phases, where the Li content is lower than or equal to the phases of interest, and r_{out} is the outer radius of this phase, a radial distribution model of the phases in the nanoparticle can be modeled. The findings are displayed in Fig. 7, which provide profound insights into the penetration of the nano-Si particles by lithium and the concomitant phase compositions of the materials.

It is evident from Fig. 7 that under the experimental charging conditions applied (0.1 C, room temperature), the lithiation of these silicon particles cannot be considered a stepwise process, where the phase with the lowest Li content is formed throughout the particle, followed by the formation of the phase with the next highest lithium, etc. Rather, the results illustrate that the migration of the lithium atoms from the surface of the nano-Si particle into the interior is too slow to result in a uniform distribution of the lithium throughout the particle. Phases with intermediate Li concentrations such as Li_7Si_3 and $Li_{13}Si_4$ are already formed at early stages in the outer regions of the particles, while the interior still contains unreacted nanosilicon. It further appears that at a certain penetration depth (here between the samples C1000 and C1500), the migration of lithium into the particle interior stops altogether, and further lithiation just changes the phase composition of the existing lithium silicides, rather than increasing particle penetration. This finding can be rationalized in view of the large volume expansion of silicon upon lithiation, thereby facilitating further lithium migration into the particles and resulting in successive phase conversions among the various Li_xSi materials formed before a uniform lithium distribution can be attained.

The NMR results also give evidence of the fundamental origins of the irreversible capacity of about 400 mAh/g detected. From the ^{6}Li MAS-NMR spectra especially from sample D-400 and consistent with the results on D-1100, C-1500, and CC-950, we can conclude that about 60% (240 mAh/g) can be ascribed to lithium in the SEI, while 40% (160 mAh/g) must be attributed to unextractable lithium in $Li_{15}Si_4$. It is possible that this part of the

irreversible capacity arises from particles in the electrode that have lost electrical contact with the current collectors during cycling, and we thus expect that this part of the irreversible capacity could potentially be eliminated by further optimizing the electrochemical cell design.

Conclusions

NMR and TEM experiments show that the electrochemical lithiation of nanosilicon particles results in core-shell materials, consisting of Li_xSi shells surrounding a core of residual silicon. While diffraction experiments indicate the absence of long-range ordering of these Li_xSi shells, solid-state NMR studies clearly reveal their chemical compositions, based on the distinct local environments of the various types of lithium species present in the shell. As such, the results give important insights into the nature of the electrochemical lithiation process: At low charging states, the formation of the SEI layer can be clearly monitored. Furthermore, lithium silicide environments with intermediate Li concentrations ($Li_{12}Si_7$, Li_7Si_3 and $Li_{13}Si_4$) can be detected at the initial stages of charging. However, at a certain penetration depth, further lithiation does not further progress toward the interior of the silicon particles but rather leads to the formation of more lithium-rich silicides with lithium contents up to the highest "nonmetallic" material $Li_{15}Si_4$.

During the delithiation, none of the low Li-containing lithium silicides is formed, and about 10% of the total charge (160 mAh/g) remains as $Li_{15}Si_4$ inside the silicon particle, while about 15% (240 mAh/g) of the total charge is irreversibly lost (SEI formation). Finally, the lithiation of the second cycle seems to be similar to the lithiation of the first cycle. The finding that only the outer few nanometers of the silicon particles are lithiated suggests that, for the improvement of silicon anodes, the reduction of the silicon particle size will be very promising for improving the capacity and performance of these anodes. Overall, the results obtained in the present study also indicate the power and potential of solid-state NMR spectroscopy for elucidating the charging/discharging mechanism of nano-Si anodes.

Acknowledgments Funding of this work by DFG project Ec168/9-1 within PAK 177 "Lithium Hochleistungsbatterien" is most gratefully acknowledged. We thank Professor Guido Schmitz for assistance with the TEM experiments and Drs. M. Miessen and P. Pilgram (Evonik, Degussa) for providing the nanosilicon materials.

References

1. Nesper R (1990) Prog Solid State Chem 20:1
2. Nesper R, von Schnering HG (1987) J Solid State Chem 70:48
3. Klemm W, Struck M (1955) Z Anorg Allg Chem 278:117
4. Boukamp BA, Lesh GC, Huggins RA (1981) J Electrochem Soc 128:725
5. Nesper R, von Schnering HG, Curda J (1986) Chem Ber 119:3576
6. Frank U, Müller W, Schäfer H (1975) Z Naturforsch B 30:10
7. von Schnering HG, Nesper R, Tebbe KF, Curda J (1980) Z Metallkunde 71:357
8. von Schnering HG, Nesper R, Curda J, Tebbe KF (1980) Angew Chem 92:1070
9. Limthongkul P, Jang Y-I, Dudney NJ, Chiang Y-M (2003) J Power Sources 119–121:604
10. Obrovac MN, Christensen L (2004) Electrochem Solid-State Lett 7:A93
11. Hatchard TD, Dahn JR (2004) J Electrochem Soc 151:A838
12. Hayes S, van Wullen L, Eckert H, Even WR, Crocker RW, Zhang Z (1997) Chem Mater 9:901
13. Dedryvère R, Olivier-Fourcade J, Jumas J (2000) Ionics 6:397
14. Dupre N, Martin J-F, Guyomard D, Yamada A, Kanno R (2008) J Mater Chem 18:4266
15. Dupré N, Martin J-F, Guyomard D, Yamada A, Kanno R (2009) J Power Sources 189:557
16. Key B, Bhattacharyya R, Morcrette M, Seznéc V, Tarascon J-M, Grey CP (2009) J Am Chem Soc 131:9239
17. Key B, Bhattacharyya R, Grey CP, Abstract of Papers, 237th ACS National Meeting (March 2009) FUEL-048, CODEN 69LNK5, AN 2009:304252
18. Stearns LA, Gryko J, Diefenbacher J, Ramachandran GK, McMillan PF (2003) J Solid State Chem 173:251
19. Dupke S, Langer T, Pöttgen R, Eckert H, manuscript in preparation
20. Xu YH, Yin GP, Zuo PJ (2008) Electrochim Acta 54:341